

# D2-MLP: Dynamic Decomposed MLP Mixer for Medical Image Segmentation

Jin Yang\*, Xiaobing Yu\*, Peijie Qiu\*

\*Mallinckrodt Institute of Radiology, Washington University School of Medicine, St. Louis, USA  
yang.jin@wustl.edu

*Abstract*—Convolutional neural networks are widely used in various segmentation tasks in medical images. However, they are challenged to learn global features adaptively due to the inherent locality of convolutional operations. In contrast, MLP Mixers are proposed as a backbone to learn global information across channels with low complexity. However, they cannot capture spatial features efficiently. Additionally, they lack effective mechanisms to fuse and mix features adaptively. To tackle these limitations, we propose a novel Dynamic Decomposed Mixer module. It is designed to employ novel Mixers to extract features and aggregate information across different spatial locations and channels. Additionally, it employs novel dynamic mixing mechanisms to model inter-dependencies between channel and spatial feature representations and to fuse them adaptively. Subsequently, we incorporate it into a U-shaped Transformer-based architecture to generate a novel network, termed the Dynamic Decomposed MLP Mixer. We evaluated it for medical image segmentation on two datasets, and it achieved superior segmentation performance than other state-of-the-art methods.

*Index Terms*—MLP Mixer, dynamic networks, medical image segmentation.

## I. INTRODUCTION

Segmentation of organs or lesions in medical images is crucial in supporting clinical workflows. However, manual segmentation is time-consuming and error-prone, thus motivating the development of automatic segmentation tools. Recently, Convolution Neural Networks (CNNs) have been widely used for automated medical image segmentation. Among CNN-based methods, U-Net and its variants are the most successful networks for medical image segmentation [1]–[5]. However, their performance is limited by the inherent locality of convolutional operations due to the challenges in learning long-range semantic information.

To overcome the inherent limitations of CNNs, the Mixer is proposed to capture long-range information based on multi-layer perceptions (MLPs), achieving a competitive performance with CNNs [6], [7]. Due to its performance and efficiency on computer vision tasks, the MLP Mixer is applied for segmentation tasks in medical images [8]–[13]. However, among these methods, some lack mechanisms to capture spatial features in basic MLP blocks, lowering the accuracy of dense predictions in medical images [9], [10], [12]. Others utilize some techniques, such as shifted MLPs or cycle MLPs, to learn spatial representations [8], [11]. However, the aggregation of information among different spatial locations

and channels is insufficient. Additionally, they lack effective mechanisms to fuse spatial and channel features adaptively.

Dynamic mechanisms have been applied to adaptively capture features [14]. Some methods employ dynamic mechanisms to adaptively aggregate features from multiple convolutional kernels based on their attention scores [15], [16]. D-Net employs dynamic mechanisms to recalibrate and fuse features from different large kernels and levels [17]. Dynamic Transformer employs a dynamic mechanism to fuse tokens from multiple windows [18]. AgileFormer employs a dynamic mechanism to capture spatial features adaptively [19]. However, few works apply dynamic mechanisms to adaptively aggregate and mix features in MLP Mixers for medical image segmentation.

To tackle these limitations, we propose a novel **Dynamic Decomposed Mixer** (DDM) module. The DDM module captures and aggregates features across different spatial locations and channels via two novel Mixers, including a **Spatially Decomposed Mixer** and a **Channel Mixer**. Specifically, our DDM module consists of three parallel paths. Two paths utilize the Spatially Decomposed Mixer to capture features and aggregate information along two different spatial dimensions, height and width, separately. It is achieved by decomposing input features into patches and rearranging them along height and width dimensions, separately. Then two MLPs are applied to capture information along with height and width, thus improving the extraction of spatial features across the whole spatial dimension. The third path employs a Channel Mixer to capture features along channels. Subsequently, the DDM module employs two dynamic mixing mechanisms, **Spatial-wise** and **Channel-wise Dynamic Mixing mechanisms** to model inter-dependencies between these channel and spatial features and to adaptively fuse them. Specifically, spatial features are extracted along two dimensions, the height and width, separately. Thus, to eliminate the isolation between these spatial features from two Spatially Decomposed Mixers, the Spatial-wise Dynamic Mixing mechanism is proposed to enhance their interactions and model inter-dependencies between spatial dimensions. The Channel-wise Dynamic Mixing mechanism is applied to adaptively fuse features from two Spatially Decomposed Mixers and the Channel Mixer.

We propose the **Dynamic Decomposed MLP Mixer** (D2-MLP) network for medical image segmentation by incorporating the DDM module into a hierarchical ViT-based encoder-

decoder architecture. It can adopt behaviors of hierarchical Vision Transformers for learning hierarchical representations efficiently. We evaluated D2-MLP on two segmentation tasks, including Abdominal Multi-organ segmentation and Liver Tumor segmentation, and it achieved superior segmentation performance than state-of-the-art models.

Our contributions have threefold: **(i)** We propose a novel Dynamic Decomposed Mixer module for learning representations. It is designed to capture features and aggregate information across different spatial locations and channels separately via the Spatially Decomposed Mixer and the Channel Mixer. Additionally, it employs novel Spatial-wise and Channel-wise Dynamic Mixing mechanisms to model inter-dependencies between spatial and channel features and to fuse them adaptively. **(ii)** We propose the Dynamic Decomposed MLP Mixer network by incorporating the Dynamic Decomposed Mixer module into a hierarchical ViT-based encoder-decoder for dense predictions. **(iii)** We evaluate the Dynamic Decomposed MLP Mixer network for medical image segmentation on two datasets. It achieved superior segmentation performance than other state-of-the-art methods.

## II. METHODOLOGY

### A. Dynamic Decomposed Mixer Module

The architecture of the DDM module is shown in Fig. 1.

1) *Spatially Decomposed Mixer*: The first two paths utilize two Spatially Decomposed Mixers to aggregate spatial information from input features  $\mathbf{X} \in \mathbb{R}^{C \times H \times W}$  ( $C$ : Channel;  $H$ : Height;  $W$ : Width) along two different spatial dimensions,  $H$  and  $W$ , separately. Most MLP-based networks aggregate information in two dimensions simultaneously along channels, leading to inefficient token interaction and inflexible information aggregation. However, our Spatially Decomposed Mixer aggregates information along two spatial dimensions separately, resulting in more flexible feature interactions across different channels.

Specifically, the Spatially Decomposed Mixer decomposes the input feature  $\mathbf{X}$  into  $N$  patches along channels, each with the dimension of  $C' \times H \times W$  (where  $C' = \frac{C}{N}$ ). The first path captures spatial features along the width  $W$ . These decomposed patches are spatially concatenated along the width  $W$  and permuted to features  $\mathbf{X}_W$  with the dimension of  $(C' * W) \times N \times H$ . Subsequently, an MLP, consisting of two linear layers, a  $1 \times 3$  depthwise convolutional layer (DWConv), and a GELU activation layer, is employed to capture features.

$$\begin{aligned}\mathbf{X}_W &= \text{Linear}(\mathbf{X}_W) \\ \mathbf{X}_W &= \text{GELU}(\text{DWConv}(\mathbf{X}_W)) \\ \mathbf{X}_W &= \text{Linear}(\mathbf{X}_W)\end{aligned}$$

In the second path, decomposed patches are spatially concatenated along the height  $H$  and permuted to features  $\mathbf{X}_H \in \mathbb{R}^{(C' * H) \times N \times W}$ . Then the Spatially Decomposed Mixer is applied to capture features along the height  $H$  by employing

an MLP, consisting of two linear layers, a  $1 \times 3$  depthwise convolutional layer, and a GELU activation.

$$\begin{aligned}\mathbf{X}_H &= \text{Linear}(\mathbf{X}_H) \\ \mathbf{X}_H &= \text{GELU}(\text{DWConv}(\mathbf{X}_H)) \\ \mathbf{X}_H &= \text{Linear}(\mathbf{X}_H)\end{aligned}$$

Then output features  $\mathbf{X}_H$  and  $\mathbf{X}_W$  are restored and transformed to the original dimension  $C \times H \times W$ .

2) *Channel Mixer*: The third path employs a Channel Mixer to capture features  $\mathbf{X}_C \in \mathbb{R}^{C \times H \times W}$  within each channel from the input  $\mathbf{X}$ . This Channel Mixer is an MLP consisting of two linear layers, a  $3 \times 3$  depthwise convolutional layer, and a GELU activation layer.

$$\begin{aligned}\mathbf{X}_C &= \text{Linear}(\mathbf{X}) \\ \mathbf{X}_C &= \text{GELU}(\text{DWConv}(\mathbf{X}_C)) \\ \mathbf{X}_C &= \text{Linear}(\mathbf{X}_C)\end{aligned}$$

3) *Spatial-wise Dynamic Mixing*: Two spatially decomposed features  $\mathbf{X}_H$  and  $\mathbf{X}_W$  are extracted along two dimensions in two isolated paths separately. Thus, we propose a Spatial-wise Dynamic Mixing mechanism to improve their interaction and model their correlations. First, we calculate the similarity score  $\mathbf{S} \in \mathbb{R}^{1 \times H \times W}$  to demonstrate the correlations between each feature in  $\mathbf{X}_H$  and spatial-wise global information  $\bar{\mathbf{X}}_W$  ( $\bar{\mathbf{X}}_W$  is derived from  $\mathbf{X}_W$  by calculating average values via pooling  $\sum_{i=1}^n \frac{x_{(w,i)}}{n}$ ). Then this similarity score  $\mathbf{S}$  is normalized and re-scaled by a Softmax function. To improve the generalizability of features  $\mathbf{X}_H$ , a tiny MLP is applied by cascading two linear layers with a GELU in between. Then the features are mixed based on their inter-dependencies dynamically as  $\mathbf{X}_H^* \in \mathbb{R}^{C \times H \times W}$ . A residual connection is also applied.

$$\begin{aligned}\mathbf{S} &= \text{Softmax}(\mathbf{X}_H \bar{\mathbf{X}}_W) \\ \mathbf{X}'_W &= \text{Linear}(\text{GELU}(\text{Linear}(\bar{\mathbf{X}}_W))) \\ \mathbf{X}_H^* &= \mathbf{X}'_W \cdot \mathbf{S} + \mathbf{X}_H\end{aligned}$$

We follow the same way to calculate  $\mathbf{X}_W^* \in \mathbb{R}^{C \times H \times W}$  from  $\mathbf{X}_W$  and spatially global information  $\bar{\mathbf{X}}_H$ .

$$\begin{aligned}\mathbf{S} &= \text{Softmax}(\mathbf{X}_W \bar{\mathbf{X}}_H) \\ \mathbf{X}'_H &= \text{Linear}(\text{GELU}(\text{Linear}(\bar{\mathbf{X}}_H))) \\ \mathbf{X}_W^* &= \mathbf{X}'_H \cdot \mathbf{S} + \mathbf{X}_W\end{aligned}$$

4) *Channel-wise Dynamic Mixing*: The Channel-wise Dynamic Mixing mechanism is applied to adaptively fuse spatial features  $\mathbf{X}_H^*$  and  $\mathbf{X}_W^*$  and channel features  $\mathbf{X}_C$ . Specifically, an adaptive average pooling is applied to calculate channel-wise significance scores  $\mathbf{W} \in \mathbb{R}^{C \times 1 \times 1}$ . Then a tiny MLP network is employed to improve the descriptions of these scores by cascading two linear layers with a GELU activation in between. A Softmax function is utilized for normalization.

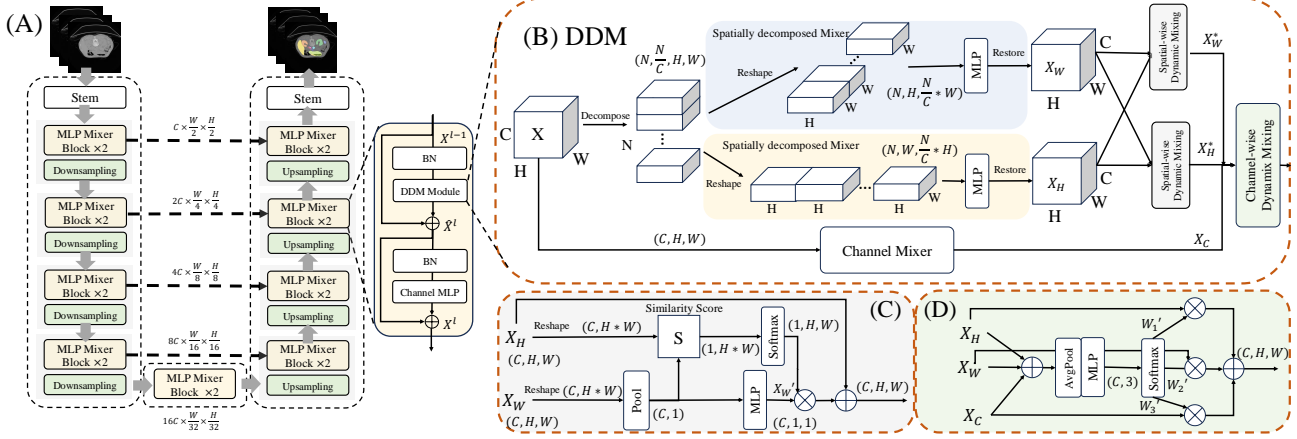


Fig. 1. (A) D2-MLP is a 4-stage encoder-decoder architecture, and each MLP Mixer block consists of a DDM module and a channel MLP. (B) The DDM module decomposes the input feature  $\mathbf{X}$  into  $N$  patches. These patches are spatially reshaped and concatenated along height  $H$  and width  $W$  to features  $\mathbf{X}_H$  and  $\mathbf{X}_W$ , separately. Subsequently, two MLPs are employed to aggregate information from  $\mathbf{X}_H$  and  $\mathbf{X}_W$  along two dimensions, separately. The interactions between  $\mathbf{X}_H$  and  $\mathbf{X}_W$  are improved in Spatial-wise Dynamic Mixing. A Channel Mixer is employed to aggregate information across channels from input features  $\mathbf{X}$  as features  $\mathbf{X}_C$ . Lastly, features  $\mathbf{X}_H^*$ ,  $\mathbf{X}_W^*$ , and  $\mathbf{X}_C$  are adaptively fused in Channel-wise Dynamic Mixing. (C) Spatial-wise Dynamic Mixing. (D) Channel-wise Dynamic Mixing.

Lastly, features are fused based on their significance scores as the output  $\mathbf{X}_{out} \in \mathbb{R}^{C \times H \times W}$ .

$$\begin{aligned} \mathbf{W} &= \text{AvgPool}(\mathbf{X}_H^* + \mathbf{X}_W^* + \mathbf{X}_C) \\ \mathbf{W}' &= \text{Linear}(\text{GELU}(\text{Linear}(\mathbf{W}))) \\ [\mathbf{W}'_1, \mathbf{W}'_2, \mathbf{W}'_3] &= \text{Softmax}(\mathbf{W}') \\ \mathbf{X}_{out} &= \mathbf{X}_H \cdot \mathbf{W}'_1 + \mathbf{X}_W \cdot \mathbf{W}'_2 + \mathbf{X}_C \cdot \mathbf{W}'_3 \end{aligned}$$

### B. MLP Mixer block

The MLP Mixer block is the basic block for representation learning in segmentation networks. It is constructed by replacing the multi-head self-attention in a standard hierarchical ViT block with the DDM module (Fig. 1). The yielded Mixer block consists of a DDM module and a Channel MLP module. A Batch Normalization (BN) layer is applied before each DDM module and Channel MLP module. A residual connection is applied after each module. Thus, the MLP Mixer block in the  $l$ -th layer can be computed as

$$\begin{aligned} \hat{\mathbf{X}}^l &= \text{DDM}(\text{BN}(\mathbf{X}^{l-1})) + \mathbf{X}^{l-1}, \\ \mathbf{X}^l &= \text{MLP}(\text{BN}(\hat{\mathbf{X}}^l)) + \hat{\mathbf{X}}^l. \end{aligned}$$

### C. Overall architecture

The D2-MLP network is designed as a 4-stage U-shaped encoder-decoder architecture for learning hierarchical feature representations (Fig. 1). In the encoder, the stem employs a  $7 \times 7$  convolutional layer with 2 strides to partition the input images and project them to  $C$  channels, thus generating features with the dimension of  $C \times \frac{H}{2} \times \frac{W}{2}$ . At each stage, two MLP Mixer blocks are stacked to perform representation learning, and a  $2 \times 2$  convolutional layer with 2 strides is employed to downscale the feature maps and increase the number of channels by a factor of 2. In the bottleneck, two consecutive MLP Mixer blocks are utilized. At each stage

of the decoder, a  $2 \times 2$  transposed convolutional layer with 2 strides is employed to upscale feature maps and decrease the number of channels by a factor of 2. Subsequently, these upsampled features are concatenated with features from the same stage of the encoder via skip connections. Two consecutive MLP Mixer blocks are then utilized. In the stem of the decoder, a  $2 \times 2$  transposed convolutional layer is employed. Lastly, a  $1 \times 1$  convolutional layer is used to produce the dense segmentation predictions. The number of feature maps at each stage is  $\{C, 2C, 4C, 8C, 16C\} = \{48, 96, 192, 384, 768\}$ .

## III. EXPERIMENTS

### A. Datasets

The first dataset is the FLARE 2021 multi-organ segmentation dataset which includes 361 multi-contrast CT images with voxel-wise manual annotations of four abdominal organs, including the liver, kidney, spleen, and pancreas [20]. The second dataset is the Medical Segmentation Decathlon (MSD) Liver tumor segmentation dataset [21]. This dataset includes 131 Portal venous phase CT images with manual annotations of liver and liver tumors.

### B. Implementation details

The D2-MLP is implemented using PyTorch. A combination of dice loss and cross-entropy loss was used as the loss function. The Stochastic Gradient Descent (SGD) was used as the optimizer. The initial learning rate was set to 0.001 and was decayed with a poly learning rate scheduler. The models were trained for 1000 epochs with deep supervision. The batch size was 14 and the input patch size was  $512 \times 512$  in two datasets. 5-fold cross-validation was utilized to split each dataset and evaluate models.

TABLE I  
COMPARISON OF SEGMENTATION PERFORMANCE BETWEEN THE D2-MLP AND OTHER SOTA APPROACHES ON THE FLARE 2021 MULTI-ORGAN SEGMENTATION DATASET AND MSD LIVER TUMOR SEGMENTATION DATASET. THE BEST RESULTS ARE LABELED BY **BOLD**. (\*:  $p < 0.01$  WITH WILCOXON SIGNED-RANK TEST BETWEEN D2-MLP AND EACH SOTA METHOD.)

Methods	Dice $\uparrow$	95HD $\downarrow$	MSD $\downarrow$	Liver $\uparrow$	Kidney $\uparrow$	Spleen $\uparrow$	Pancreas $\uparrow$	Dice $\uparrow$	95HD $\downarrow$	MSD $\downarrow$	Liver $\uparrow$	Tumor $\uparrow$
Att U-Net	91.61	4.71	1.04	97.81	96.07	<b>97.15</b>	75.43	73.10	16.96	5.33	94.71	51.49
nnU-Net	91.54	4.74	1.05	97.83	96.06	97.14	75.14	72.50	19.49	7.90	94.49	50.51
DconnNet	91.42	4.93	1.10	97.62	95.55	96.94	75.57	72.80	19.53	7.22	94.45	51.15
Swin U-Net	87.86	7.62	1.72	96.82	93.60	95.74	65.28	65.16	38.50	14.45	92.73	37.59
MISSFormer	90.94	5.94	1.34	97.48	95.39	96.46	74.43	71.93	26.25	9.33	94.15	49.71
UTNet	89.20	6.68	1.47	97.32	94.94	96.52	68.03	71.16	21.26	9.50	93.85	48.47
UCTransNet	91.84	4.93	1.09	97.81	96.10	96.81	76.63	72.04	21.14	7.59	93.81	50.27
HiFormer	90.17	7.14	1.73	97.13	94.89	95.43	73.22	71.71	26.57	9.63	93.94	49.60
UNeXt	89.09	7.04	1.56	96.90	94.53	95.83	69.12	71.70	22.63	8.73	93.69	49.70
D2-MLP	<b>92.53*</b>	<b>3.99*</b>	<b>1.02*</b>	<b>98.21</b>	<b>96.39</b>	96.52	<b>79.00</b>	<b>75.73*</b>	<b>15.25*</b>	<b>4.93*</b>	<b>95.37</b>	<b>56.10</b>

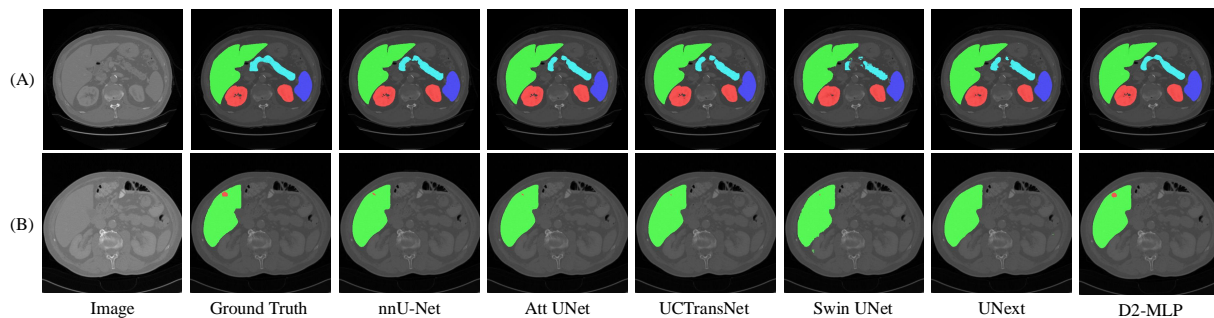


Fig. 2. Qualitative comparison between D2-MLP and other methods in (A) the FLARE Multi-organ and (B) MSD Liver Tumor datasets.

TABLE II  
THE COMPARISON OF PERFORMANCE AMONG VARIOUS DESIGNS OF THE D2-MLP METHOD ON THE FLARE MULTI-ORGAN SEGMENTATION DATASET. THE BEST DICE SCORES ARE LABELED BY **BOLD**.

Models	Average	Liver	Kidney	Spleen	Pancreas
$N = 2$	91.29	96.71	93.93	95.14	79.36
$N = 4$	<b>92.53</b>	<b>98.21</b>	<b>96.39</b>	<b>96.52</b>	79.00
$N = 8$	92.36	97.85	95.95	95.75	<b>79.90</b>
$N = 16$	90.38	96.95	94.22	93.67	76.67
Basic Mixer	88.36	94.64	93.02	92.58	73.22
DDM	92.53	98.21	96.39	96.52	79.00

### C. Experimental results

To evaluate the model performance, we employed the Dice coefficient (Dice), 95th Percentile Hausdorff Distance (95HD), and Mean Surface Distance (MSD) as evaluation metrics. To implement a thoughtful comparison, we compared D2-MLP with various 2D SOTA models, including CNN-based models (Attention U-Net [22], nnU-Net [23], and DconnNet [24]), ViT-based models (Swin U-Net [25] and MISSFormer [26]), hybrid ViT-CNN models (UTNet [27], UCTransNet [28], and HiFormer [29]), and a MLP-based model (UNeXt [8]). Table I shows that the D2-MLP network achieved superior overall performance over other SOTA methods on both two segmentation tasks. The D2-MLP model showed significant improvement across almost all organ-specific segmentation tasks. The qualitative comparison shows that D2-MLP achieved better results than other SOTA methods (Fig. 2).

### D. Ablation study on Dynamic Decomposed Mixer module

1) *The impact of patch number*: We conducted an ablation study to investigate the impact of the patch number  $N$  on model performance. Table II shows that the D2-MLP achieved the best segmentation performance when the patch number is 4 ( $N = 4$ ). It achieved the second-best performance when the patch number is 8 ( $N = 8$ ).

2) *The effectiveness of DDM module*: In this study, we evaluated the effectiveness of the DDM module on medical image segmentation by replacing it with a basic Channel Mixer module in D2-MLP. Table II demonstrates that D2-MLP with the DDM module achieved a much higher Dice score than that with a basic Mixer module, showing its effectiveness on medical image segmentation.

## IV. CONCLUSIONS

We propose a Dynamic Decomposed MLP Mixer network for medical image segmentation. This network employs a Dynamic Decomposed Mixer module to learn spatial and channel features and aggregate them adaptively. The experimental results demonstrate the superior performance of our segmentation model over other SOTA methods and the benefits of the Dynamic Decomposed Mixer module on segmentation.

## REFERENCES

- [1] O. Ronneberger, P. Fischer, and T. Brox, "U-net: Convolutional networks for biomedical image segmentation," in *Medical image computing and computer-assisted intervention—MICCAI 2015: 18th international conference, Munich, Germany, October 5-9, 2015, proceedings, part III 18*, pp. 234–241, Springer, 2015.

- [2] Ö. Çiçek, A. Abdulkadir, S. S. Lienkamp, T. Brox, and O. Ronneberger, "3d u-net: learning dense volumetric segmentation from sparse annotation," in *Medical Image Computing and Computer-Assisted Intervention–MICCAI 2016: 19th International Conference, Athens, Greece, October 17–21, 2016, Proceedings, Part II 19*, pp. 424–432, Springer, 2016.
- [3] Z. Zhou, M. M. Rahman Siddiquee, N. Tajbakhsh, and J. Liang, "Unet++: A nested u-net architecture for medical image segmentation," in *Deep Learning in Medical Image Analysis and Multimodal Learning for Clinical Decision Support: 4th International Workshop, DLMIA 2018, and 8th International Workshop, ML-CDS 2018, Held in Conjunction with MICCAI 2018, Granada, Spain, September 20, 2018, Proceedings 4*, pp. 3–11, Springer, 2018.
- [4] J. Yang, D. S. Marcus, and A. Sotiras, "Abdominal ct pancreas segmentation using multi-scale convolution with aggregated transformations," in *Medical Imaging 2023: Computer-Aided Diagnosis*, vol. 12465, pp. 416–424, SPIE, 2023.
- [5] J. Yang, D. S. Marcus, and A. Sotiras, "Dynamic u-net: Adaptively calibrate features for abdominal multi-organ segmentation," *arXiv preprint arXiv:2403.07303*, 2024.
- [6] I. O. Tolstikhin, N. Houlsby, A. Kolesnikov, L. Beyer, X. Zhai, T. Unterthiner, J. Yung, A. Steiner, D. Keysers, J. Uszkoreit, et al., "Mlp-mixer: An all-mlp architecture for vision," *Advances in neural information processing systems*, vol. 34, pp. 24261–24272, 2021.
- [7] G. Cao, S. Luo, W. Huang, X. Lan, D. Jiang, Y. Wang, and J. Zhang, "Strip-mlp: Efficient token interaction for vision mlp," in *Proceedings of the IEEE/CVF International Conference on Computer Vision*, pp. 1494–1504, 2023.
- [8] J. M. J. Valanarasu and V. M. Patel, "Unext: Mlp-based rapid medical image segmentation network," in *International conference on medical image computing and computer-assisted intervention*, pp. 23–33, Springer, 2022.
- [9] S. Pan, C.-W. Chang, T. Wang, J. Wynne, M. Hu, Y. Lei, T. Liu, P. Patel, J. Roper, and X. Yang, "Abdomen ct multi-organ segmentation using token-based mlp-mixer," *Medical Physics*, vol. 50, no. 5, pp. 3027–3038, 2023.
- [10] J. Pang, C. Jiang, Y. Chen, J. Chang, M. Feng, R. Wang, and J. Yao, "3d shuffle-mixer: An efficient context-aware vision learner of transformer-mlp paradigm for dense prediction in medical volume," *IEEE Transactions on Medical Imaging*, 2022.
- [11] Y. Liu, H. Zhu, M. Liu, H. Yu, Z. Chen, and J. Gao, "Rolling-unet: Revitalizing mlp's ability to efficiently extract long-distance dependencies for medical image segmentation," in *Proceedings of the AAAI Conference on Artificial Intelligence*, vol. 38, pp. 3819–3827, 2024.
- [12] Z. Zhou, M. T. Islam, and L. Xing, "Multibranch cnn with mlp-mixer-based feature exploration for high-performance disease diagnosis," *IEEE Transactions on Neural Networks and Learning Systems*, 2023.
- [13] J.-H. Shi, Q. Zhang, Y.-H. Tang, and Z.-Q. Zhang, "Polyp-mixer: An efficient context-aware mlp-based paradigm for polyp segmentation," *IEEE Transactions on Circuits and Systems for Video Technology*, vol. 33, no. 1, pp. 30–42, 2022.
- [14] Y. Han, G. Huang, S. Song, L. Yang, H. Wang, and Y. Wang, "Dynamic neural networks: A survey," *IEEE Transactions on Pattern Analysis and Machine Intelligence*, vol. 44, no. 11, pp. 7436–7456, 2021.
- [15] Y. Chen, X. Dai, M. Liu, D. Chen, L. Yuan, and Z. Liu, "Dynamic convolution: Attention over convolution kernels," in *Proceedings of the IEEE/CVF conference on computer vision and pattern recognition*, pp. 11030–11039, 2020.
- [16] X. Li, W. Wang, X. Hu, and J. Yang, "Selective kernel networks," in *Proceedings of the IEEE/CVF conference on computer vision and pattern recognition*, pp. 510–519, 2019.
- [17] J. Yang, P. Qiu, Y. Zhang, D. S. Marcus, and A. Sotiras, "D-net: Dynamic large kernel with dynamic feature fusion for volumetric medical image segmentation," *arXiv preprint arXiv:2403.10674*, 2024.
- [18] P. Ren, C. Li, G. Wang, Y. Xiao, Q. Du, X. Liang, and X. Chang, "Beyond fixation: Dynamic window visual transformer," in *Proceedings of the IEEE/CVF Conference on Computer Vision and Pattern Recognition*, pp. 11987–11997, 2022.
- [19] P. Qiu, J. Yang, S. Kumar, S. S. Ghosh, and A. Sotiras, "Agileformer: Spatially agile transformer unet for medical image segmentation," *arXiv preprint arXiv:2404.00122*, 2024.
- [20] J. Ma, Y. Zhang, S. Gu, C. Zhu, C. Ge, Y. Zhang, X. An, C. Wang, Q. Wang, X. Liu, et al., "Abdomenct-1k: Is abdominal organ segmen-
- tation a solved problem?," *IEEE Transactions on Pattern Analysis and Machine Intelligence*, vol. 44, no. 10, pp. 6695–6714, 2021.
- [21] M. Antonelli, A. Reinke, S. Bakas, K. Farahani, A. Kopp-Schneider, B. A. Landman, G. Litjens, B. Menze, O. Ronneberger, R. M. Summers, et al., "The medical segmentation decathlon," *Nature communications*, vol. 13, no. 1, p. 4128, 2022.
- [22] J. Schlemper, O. Oktay, M. Schaap, M. Heinrich, B. Kainz, B. Glocker, and D. Rueckert, "Attention gated networks: Learning to leverage salient regions in medical images," *Medical image analysis*, vol. 53, pp. 197–207, 2019.
- [23] F. Isensee, P. F. Jaeger, S. A. Kohl, J. Petersen, and K. H. Maier-Hein, "nnu-net: a self-configuring method for deep learning-based biomedical image segmentation," *Nature methods*, vol. 18, no. 2, pp. 203–211, 2021.
- [24] Z. Yang and S. Farsiu, "Directional connectivity-based segmentation of medical images," in *Proceedings of the IEEE/CVF conference on computer vision and pattern recognition*, pp. 11525–11535, 2023.
- [25] H. Cao, Y. Wang, J. Chen, D. Jiang, X. Zhang, Q. Tian, and M. Wang, "Swin-unet: Unet-like pure transformer for medical image segmentation," in *European conference on computer vision*, pp. 205–218, Springer, 2022.
- [26] X. Huang, Z. Deng, D. Li, X. Yuan, and Y. Fu, "Missformer: an effective transformer for 2d medical image segmentation," *IEEE transactions on medical imaging*, 2022.
- [27] Y. Gao, M. Zhou, and D. N. Metaxas, "Utnet: a hybrid transformer architecture for medical image segmentation," in *Medical Image Computing and Computer Assisted Intervention–MICCAI 2021: 24th International Conference, Strasbourg, France, September 27–October 1, 2021, Proceedings, Part III 24*, pp. 61–71, Springer, 2021.
- [28] H. Wang, P. Cao, J. Wang, and O. R. Zaiane, "Uctransnet: rethinking the skip connections in u-net from a channel-wise perspective with transformer," in *Proceedings of the AAAI conference on artificial intelligence*, vol. 36, pp. 2441–2449, 2022.
- [29] M. Heidari, A. Kazerouni, M. Soltany, R. Azad, E. K. Aghdam, J. Cohen-Adad, and D. Merhof, "Hiformer: Hierarchical multi-scale representations using transformers for medical image segmentation," in *Proceedings of the IEEE/CVF winter conference on applications of computer vision*, pp. 6202–6212, 2023.